Biophysical *Journal*
Article

Biophysical Society

The Selectivity Filter Is Involved in the U-Type Inactivation Process of Kv2.1 and Kv3.1 Channels

Laura Coonen,[1] Evy Mayeur,[1] Nicolas De Neuter,[1] Dirk J. Snyders,[1] Luis G. Cuello,[2] and Alain J. Labro[1,*]
[1]Laboratory for Molecular, Cellular and Network Excitability, University of Antwerp, Antwerp, Belgium and [2]Cell Physiology and Molecular Biophysics, Center for Membrane Protein Research, Texas Tech University Health Sciences Center, Lubbock, Texas

ABSTRACT Voltage-gated potassium (Kv) channels display several types of inactivation processes, including N-, C-, and U-types. C-type inactivation is attributed to a nonconductive conformation of the selectivity filter (SF). It has been proposed that the activation gate and the channel's SF are allosterically coupled because the conformational changes of the former affect the structure of the latter and vice versa. The second threonine of the SF signature sequence (e.g., TTVGYG) has been proven to be essential for this allosteric coupling. To further study the role of the SF in U-type inactivation, we substituted the second threonine of the TTVGYG sequence by an alanine in the hKv2.1 and hKv3.1 channels, which are known to display U-type inactivation. Both hKv2.1-T377A and hKv3.1-T400A yielded channels that were resistant to inactivation, and as a result, they displayed noninactivating currents upon channel opening; i.e., hKv2.1-T377A and hKv3.1-T400A remained fully conductive upon prolonged moderate depolarizations, whereas in wild-type hKv2.1 and hKv3.1, the current amplitude typically reduces because of U-type inactivation. Interestingly, increasing the extracellular K^+ concentration increased the macroscopic current amplitude of both hKv2.1-T377A and hKv3.1-T400A, which is similar to the response of the homologous T to A mutation in *Shaker* and hKv1.5 channels that display C-type inactivation. Our data support an important role for the second threonine of the SF signature sequence in the U-type inactivation gating of hKv2.1 and hKv3.1.

SIGNIFICANCE Voltage-dependent K^+ (Kv) channels generate cells' repolarizing power, which is consequently regulated by the channel's conductance. Aside from the opening or closure, Kv channels undergo inactivation that drives them into a lower or nonconductive state. Among the different inactivation processes described in Kv channels, the U-type process develops from a preopen but activated state. The molecular determinants of this process are, in contrast to the C-type mechanism, not well characterized. Our data show that the intracellular part of the K^+ selectivity filter within the pore domain is involved. An alanine for threonine substitution results in channels that do not inactivate upon opening, suggesting that an allosteric coupling between the activation gate and selectivity filter exists in U-type inactivation.

INTRODUCTION

Voltage-gated potassium (Kv) channels are responsible for the voltage-controlled efflux of K^+ ions (1). Based on their amino-acid sequence, the large Kv channel family is divided into 10 subfamilies (2). The members of the Kv2 (*Shab*-related, KCNB1-2) and Kv3 (*Shaw*-related, KCNC1-4) subfamilies are mostly delayed rectifying channels, i.e., they display depolarization-activated currents that inactivate slowly. Although the gating behavior differs between Kv channels, in most cases the channel transitions through the closed (*C*), open (*O*), open-inactivated (*I*), and closed-inactivated (*CI*) states (Fig. 1; (3)).

Kv channels typically consist of four identical subunits, each composed of six transmembrane helices (S1–S6) with a membrane reentering P-loop between S5 and S6 (1,4). The four subunits assemble such that the S5-P-S6 regions form the channel's K^+ conductive pore, which is surrounded by four voltage-sensing domains (VSDs) composed of the S1–S4 helices. The pore contains toward its extracellular end a selectivity filter (SF), which is constituted by the TTVGYG signature sequence of K^+ channels (5). The backbone carbonyl groups from this structural motif together with the OH-side chain of the second threonine of this TTVGYG motif create four distinct K^+ binding sites (6). The pore also contains structural gates that control the K^+ flow. It is generally accepted that the channel's

Submitted October 28, 2019, and accepted for publication March 25, 2020.
*Correspondence: alain.labro@uantwerpen.be
Editor: Baron Chanda.
https://doi.org/10.1016/j.bpj.2020.03.032

FIGURE 1 Sequence homology of Kv subfamily members with minimal gating diagram. (*a*) shows the sequence alignment of the P-loop (contributing to the SF) in KcsA, *Shaker*, hKv1.5, hKv2.1, and hKv3.1. The second threonine residue within this filter (*indicated in bold*) is replaced by alanine in this work. (*b*) depicts a minimal gating diagram with six states whereby the activated (A) and activated-inactivated (AI) states are intermediate states that the channel transitions to go from closed to open or inactivated and vice-versa. In the nonconductive closed state (C), the SF (S) has an open conformation, whereas the intracellular AG gate (G) is closed. Upon membrane depolarization, the AG converts into an activated and subsequently an open conformation, and the ion channel is conductive (O state). In channels displaying C-type inactivation, prolonged depolarization causes the channel to inactivate (I state) through SF rearrangements and ion conduction is inhibited. Finally, upon closing of the activation gate during repolarization, the channel occupies the closed-inactivated state (CI).

voltage-controlled activation gate (AG) is located at the cytoplasmic end of the S6 helix, also known as the bundle crossing point (6,7). The opening and closure of the channel's AG is structurally and functionally coupled to the movement of the VSDs (8), a process known as the electromechanical coupling (9).

The SF not only determines K^+ selectivity but also regulates ion channel permeation properties (10). In the well-studied open-state C-type inactivation process (11), the SF undergoes conformational changes and becomes nonconductive after the AG has opened (12–16). Because the conduction properties of the SF depend on the status of the AG, it is said that they are allosterically coupled (17–22). In other words, the conformation of the AG affects the structure and hence the SF's functional state in a bidirectional fashion (23,24). Functional studies on the *Shaker* and the human *Shaker*-type hKv1.5 channel have identified the second threonine residue of the TTVGYG motif as an important determinant for the coupling between the AG opening and the channel's SF (25). Substituting this threonine by an alanine residue inverted this allosteric coupling between both structural motifs, yielding a SF that is inactive when the AG is closed but becomes conductive upon opening of the AG, hence resetting it to the conductive conformation.

U-type inactivation manifests itself by the channel's preference to inactivate from a preopen yet nonconductive state (26,27). Consequently, the degree of channel inactivation is less pronounced at more depolarized potentials, resulting in a U-shaped voltage-dependent inactivation profile. Deleting parts of the N-terminus in hKv1.5 resulted in mutant channels displaying U-type inactivation (28). Also, in the *Shaker* channel, U-type inactivation is present at moderated depolarizations (26) or by mutations at the residue T449, near the outer K^+ binding site of the SF (29). Thus, U- and C-type inactivation processes can coexist, but one is usually phenotypically the dominant (30).

Currently, a structural view of the C-type inactivation process involves structural rearrangements at the channel SF that eventually caused the cessation of ion permeation. However, the molecular determinants of U-type inactivation are less characterized. A role for the SF in C-type inactivation was proposed upon the observation that elevated extracellular $[K^+]$ slows it (31–33) and that the channel's ion selectivity changes upon inactivation (34,35). In U-type inactivation, on the other hand, channel inactivation develops faster when extracellular $[K^+]$ is elevated (26,27). However, the recovery from U-type inactivation responds similarly and, in both C- and U-type, is accelerated by increased extracellular $[K^+]$ (27,36). Furthermore, as in C-type inactivation, the changes of ion selectivity displayed by U-type inactivated Kv2.1 channels suggest a role for the SF in also U-type inactivation (34). This notion is supported by the observation that replacing the P-loop of Kv2.1 by the one from Kv1.3 (in which C-type inactivation dominates) yielded a chimeric Kv2.1-Kv1.3 channel that displayed C-type inactivation properties (37). Here, we explore whether the internal part of the channel's SF participates in the U-type inactivation process. We tested this idea by substituting the second threonine residues within the TTVGYG motif with an alanine in Kv channels in which U-type inactivation is dominant (Fig. 1), such as the human hKv2.1 and the hKv3.1 channel (26,27).

MATERIALS AND METHODS

Creating channel mutants, molecular biology

hKv2.1 and hKv3.1 complementary DNA (cDNA) were cloned in pBK-CMV and peGFP-N1 vector for expression in Ltk- cells, respectively. T to A mutations were introduced through site-directed mutagenesis using the QuickChange site-directed mutagenesis kit (Stratagene, La Jolla, CA) and primers containing the desired mutation. Sufficient plasmid DNA was obtained by amplification in XL2-blue ultracompetent *Escherichia coli* bacteria (Agilent Technologies, Santa Clara, CA), followed by plasmid purification using the NucleoBond Xtra Maxi kit (Machery-Nagel, Düren, Germany). Presence of the desired T to A mutations and absence of unwanted mutations was confirmed through Sanger sequencing (performed at the VIB Genetic Sequencing Facility, Antwerp, Belgium).

Cell culture, transfection, and electrophysiology

Kv channels were transiently expressed in Ltk cells by transfecting subconfluent cell culture dishes with 10–20 ng of plasmid cDNA using lipofectamine 2000 (Thermo Fisher Scientific, MA). To compensate for low current expression of the mutant channels, the amount of cDNA transfected was increased up to a maximum of 5 μg per 60 × 15-mm cell culture dish. Cells were harvested 24 h post-transfection using a Gibco 0.05% trypsin-EDTA solution (Thermo Fisher Scientific). Whole-cell ionic current measurements were performed at room temperature using an axopatch 200b amplifier, and recordings were digitized with a digidata 1440 (Molecular Devices, San Jose, CA). Recordings were sampled at 2–10 kHz after passing through a 1- to 5-kHz low-pass filter. Cells were continuously

superfused with a standard extracellular solution: NaCl 130 mM, KCl 4 mM, $CaCl_2$ 1.8 mM, $MgCl_2$ 1 mM, HEPES 10 mM, and glucose 10 mM (adjusted to pH 7.35 with NaOH). External solutions with elevated K^+ concentration, used to accelerate the conversion from the inactivated state to the conducting one, were obtained by replacing NaCl with KCl. Fast switching between different external solutions was achieved using a pressurized fast-perfusion system (custom built with electrofluidic valves purchased from Lee Products, Buckinghamshire, UK). Patch pipettes were pulled from borosilicate glass with a P-2000 puller (Sutter Instruments, Navato, CA) and afterwards heat polished, resulting in pipette resistances of 1–2 MΩ. The pipettes were filled with an intracellular solution: KCl 110 mM, NaCl 1 mM, K_4BAPTA 5 mM, K_2ATP 5 mM, $MgCl_2$ 1 mM, and HEPES 10 mM (adjusted to pH 7.2 with KOH). Applied pulse protocols are shown in the figures.

Data analysis

The data were analyzed with Pclamp10 software (Molecular Devices), and shown figures were made with Sigmaplot (Systat Software, Santa Clara, CA). Data were excluded when the estimated voltage error exceeded 5 mV after series resistance compensation. All conductance-voltage curves were fitted with a single Boltzmann equation: $y = 1/\{1 + \exp[-(V - V_{1/2})/k]\}$, with V as the applied voltage, $V_{1/2}$ as the voltage at which half of the channels are opened or inactivated, and k as the slope factor. Time constants of activation were obtained by fitting the rising phase of the macroscopic current activations from recordings shown in Fig. 2, *a* and *b* with a single-exponential function. The deactivation time constants were obtained from fitting the current decay upon different repolarizing potentials from recordings shown in Fig. 3, *a* and *b* with a single- or double-exponential function. Permeability ratios for Na^+/K^+ were determined in the standard extracellular and intracellular recording solutions from the reversal potential ($V_{reversal}$, obtained using deactivation pulse protocols shown in Fig. 3) using the Goldman-Hodgkin-Katz equation. All data are represented as average values ± standard error of the mean (SEM), with n the number of cells analyzed.

Single-channel conductance was estimated with nonstationary noise analysis. Whole-cell activating currents were recorded with a pulse protocol that consisted of 60 repetitive pulses to +40 mV. Only cells that did not display current rundown during the train of pulses were used for analysis. Current recordings were analyzed using the built-in nonstationary fluctuation analysis tool of Pclamp10 software. This analysis tool calculates the ensemble current variance (σ^2) of the different tracings and plots it as a function of total current. This relation was then approximated with the parabolic function $\sigma^2 = iI - I^2/n + c$, where i is the single-channel current, I is the total current, n is the number of channels, and c is a constant background current (*offset*). Subsequently, the single-channel conductance (γ) was calculated from the obtained single-channel current i.

RESULTS

hKv2.1 and hKv3.1 are human orthologs of the drosophila *Shab* and *Shaw* subfamily and belong to the larger *Shaker*-type-related Kv family. Both channels are activated upon depolarization and display current inactivation. In contrast to *Shaker* and hKv1.5 channels, hKv2.1 and hKv3.1 are reported to display U-type inactivation (26,27). Substituting the second threonine of the TTVGYG motif with alanine in hKv2.1 and hKv3.1 yielded the channel mutants hKv2.1-T377A and hKv3.1-T400A, respectively (Fig. 1). When expressed in Ltk cells, both mutants generated functional channels that

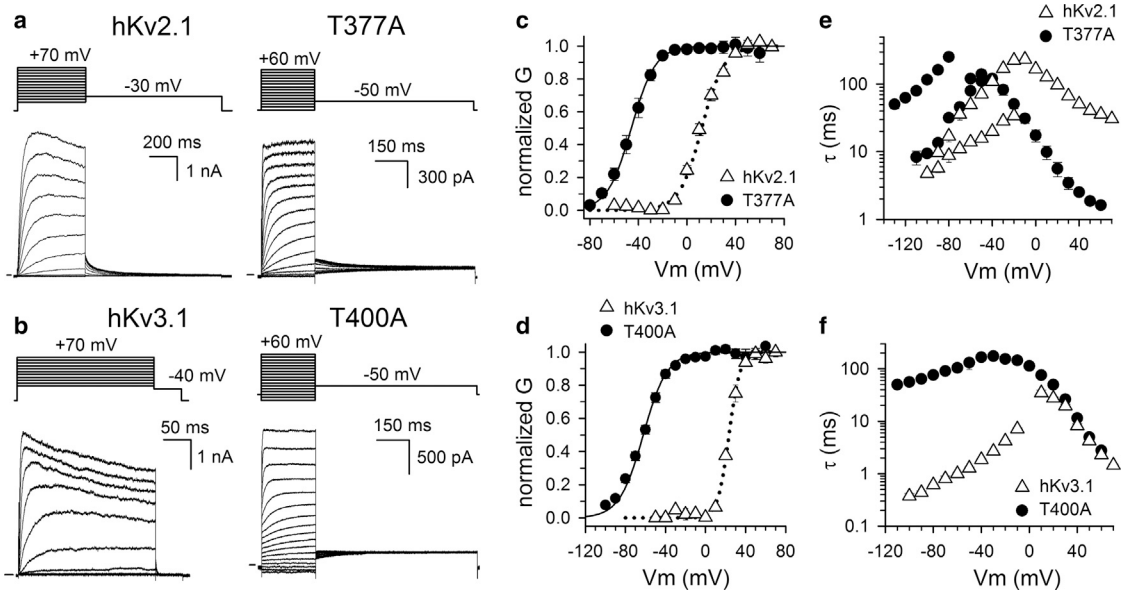

FIGURE 2 Activation kinetics of WT hKv2.1 and hKv3.1 and the alanine mutations hKv2.1-T377A and hKv3.1-T400A. Representative whole-cell current recordings of Ltk cells expressing WT channels or their corresponding T-to-A mutations, hKv2.1 (*a*) and hKv3.1 (*b*), are shown. Currents were elicited with the pulse protocols shown on top, and the horizontal bar at the start of the recordings indicates the zero-current level. After applying activating depolarizing pulses, the membrane potential was stepped back to a fixed value to elicit deactivating tail currents. Shown in (*c*) and (*d*) are the voltage dependence of activation for the hKv2.1 and hKv3.1 channels (*open triangles*) and their corresponding T-to-A mutations (*solid circles*). The conductance (G) versus voltage (V) relationship or GV curves were obtained by plotting the normalized G (obtained by normalizing the tail current amplitudes from pulse protocols shown in *a* and *b*) as a function of the voltage changes. Values are the means ± SEM with solid and dotted lines representing the average fit with a Boltzmann function ($V_{1/2}$ and slope factor values are reported in Table 1). (*e*) and (*f*) display the activation and deactivation time constants for the WT channels (*open triangles*), hKv2.1 (*e*) and hKv3.1 (*f*). The time constants of the mutants hKv2.1-T377A and hKv3.1-T400A were obtained in a similar manner and are displayed with black symbols.

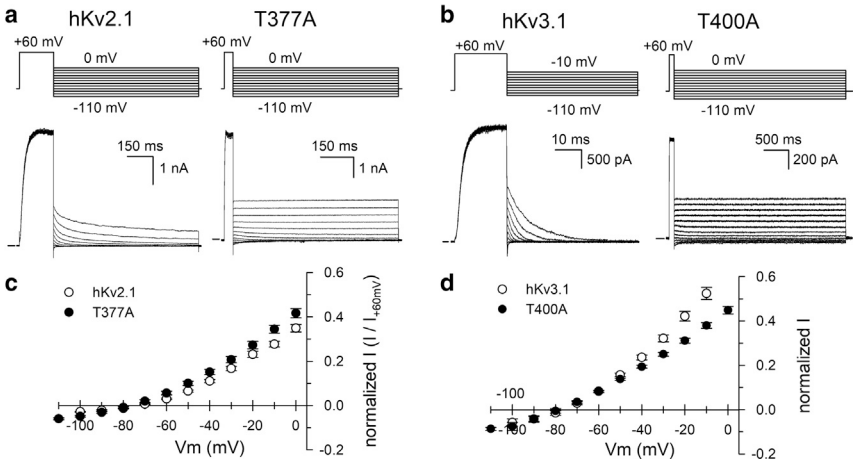

FIGURE 3 hKv2.1-T377A and hKv3.1-T400A produced K^+ selective channels. (*a*) and (*b*) show representative current recordings for hKv2.1 and its T377A mutation (*a*) and for hKv3.1 and its T400A mutation (*b*), respectively. Currents were elicited with the pulse protocol shown at the top, and the horizontal bar at the start of the recordings indicates the zero-current level. (*c*) and (*d*) show current (I) versus voltage curves (*IV curves*) that were obtained by plotting the normalized amplitude of the deactivating currents from recordings shown in (*a*) and (*b*) (normalized to the current amplitude at +60 mV) as a function of repolarizing potential. The IV curves of both hKv2.1-T377A and hKv3.1-T400A (*solid circles*) were comparable to those of the WT channels (*open circles*). WT and mutant channels displayed a similar reversal potential, i.e., the potential where the current is 0.

displayed voltage-dependent current activation and deactivation (Fig. 2). Their conductance-versus-voltage (GV) relationship indicated that in both hKv2.1 and hKv3.1, the T to A substitution shifted the voltage dependency of channel activation toward more hyperpolarized potentials (Fig. 2). Both hKv2.1-T377A and hKv3.1-T400A displayed approximately a −60 and −80 mV hyperpolarizing shift in their midpoint of activation ($V_{1/2}$ values) compared with wild-type (WT) channels (Table 1). In the case of hKv3.1-T400A, the slope of the curve also became shallower. Taking these shifts in the voltage dependence of activation into account, hKv2.1-T377A displayed kinetics similar to WT hKv2.1 (Fig. 2). On the other hand, the deactivation kinetics of hKv3.1-T400A were about 100-fold slower compared to the WT (Fig. 2).

Previously, it was shown that an alanine substitution of the second threonine residue of the signature sequence of the *Shaker* and hKv1.5 channels affected their conduction properties but did not change their K^+ over Na^+ selectivity (25). Remarkably, the hKv2.1-T377A and hKv3.1-T400A mutants remained highly K^+ over Na^+ selective, similar to the WT channels (Table 1). The K^+ over Na^+ selectivity of the WT and the mutant channels was calculated from the current reversal potential that was determined by creating the current-voltage (IV) curves of fully open channels using the pulse protocol displayed in Fig. 3. With the solutions used in these experiments, the reversal potential was around −75 mV for both WT and mutant channels (Fig. 3; Table 1).

TABLE 1 GV Curve, Ion Selectivity, and Unitary Conductance Properties of WT and Mutant Channels, with *n* the Number of Cells Analyzed

	GV Curve		Selectivity			
	$V_{1/2}$ (mV)	Slope k	Ratio Na^+/K^+	*n*	γ (pS)	*n*
WT Kv2.1	12.2 ± 1.4	9.5 ± 0.6	0.015 ± 0.004	7	10.3 ± 0.4	3
T377A	−45.8 ± 2.4	9.9 ± 0.6	0.010 ± 0.002	6	4.9 ± 0.3	3
WT Kv3.1	23.5 ± 1.0	5.6 ± 0.3	0.014 ± 0.003	6	24.1 ± 3.1	3
T400A	−62.2 ± 2.9	11.9 ± 1.1	0.013 ± 0.002	5	5.6 ± 0.6	3

Because this value is close to the Nernst equilibrium potential for K^+ in these experimental conditions, this indicates that the mutant channels are WT-like K^+ selective. To evaluate the unitary channel conductance of hKv2.1-T377A and hKv3.1-T400A, we performed a nonstationary noise analysis (Fig. 4). The resultant conductance for the WT hKv2.1 and hKv3.1 channels agrees with previously reported values (38–42). However, for both Kv2.1-T377A and Kv3.1-T400A, their unitary channel conductance dropped about two- and fourfold, respectively (when compared to the WT channel, Table 1).

Upon prolonged 5-s depolarizations, the current amplitude of WT hKv2.1 gradually decreased, indicating that the channels underwent inactivation (Fig. 5). Measuring inactivation after 5 s to different potentials yielded the typical U-shape profile of the voltage dependence of channel inactivation. Interestingly, the fraction of inactivated channels first increases as the membrane depolarization becomes more positive, reaching a plateau at a membrane potential of ∼0 mV. At depolarizations above 0 mV, a clear reduction of the fraction of inactivated channels was observed, which generated the U-shape profile (Fig. 6). In the hKv2.1-T377A mutant, 5-s depolarizations did not cause marked inactivation (Fig. 5). Moreover, 5-s depolarization at +20 mV induced a noticeable increase in current of ∼13 ± 3% (n = 7). This is opposite of what is observed in WT hKv2.1, in which a 5-s depolarization at +20 mV decreases the current amplitude by ∼44 ± 4% (n = 5) because of channel inactivation. Consequently, the hKv2.1-T377A mutant did not display a U-shape inactivation curve as did WT hKv2.1 and seemed reluctant to inactivate (Fig. 6). Even if there was a change in conductivity upon 5-s depolarization, the current amplitude displayed an increasing trend in the voltage range between −60 and −20 mV, and only at stronger depolarizations, which in WT channels relieves inactivation, could a small decrease in current be observed. To explain the increasing trend in current amplitude, the presence of closed-state inactivation was evaluated. Unlike

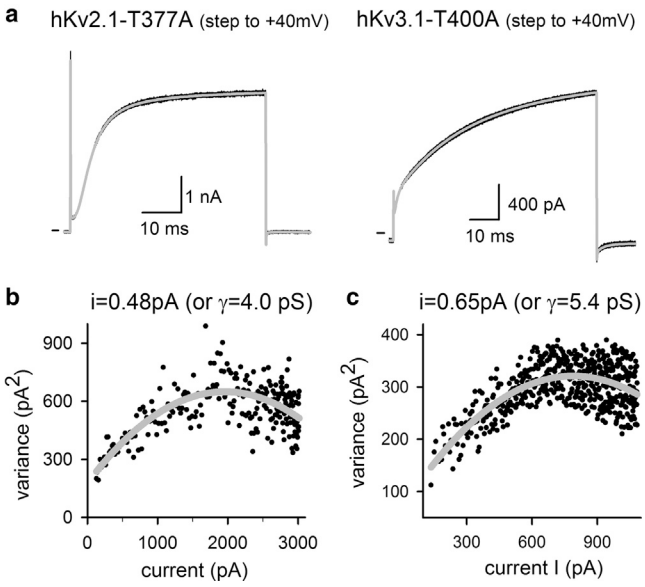

FIGURE 4 Noise analysis of hKv2.1-T377A and hKv3.1-T400A to determine channel conductance. (*a*) shows the representative current recordings of hKv2.1-T377A (*left*) and hKv3.1-T400A (*right*) elicited by repetitively applying a +40-mV pulse. The gray trace is the calculated average. (*b*) and (*c*) plot the calculated variance, obtained from analyzing the upstroke of the activating current recordings shown in (*a*), as a function of current amplitude. Fitting these relationships with a parabolic function (*gray tracing*) yielded a single-channel current i of 0.48 pA for hKv2.1-T377A (*b*) and 0.65 pA for hKv3.1-T400A (*c*), respectively. These single-channel currents correspond to a single-channel conductance γ, represented in parentheses.

observed in Kv1.5-T480A and *Shaker*-T442A, closed-state inactivation that is relieved by AG opening was not obviously present in hKv2.1-T377A (Fig. S1).

hKv3.1 also displays a robust current inactivation upon 5-s depolarizations (Fig. 5). Consequently, only 39 ± 3% (n = 3) of the peak current remained after a 5-s conditioning pulse to +30 mV. A hallmark of U-type inactivation is that the amount of inactivation is less pronounced at more depolarized potentials (i.e., above +40 mV). Thus, a U-shape inactivation behavior is observed when plotting the voltage dependence of inactivation (Fig. 6). Applying similar 5-s depolarizations to the hKv3.1-T400A mutant elicited noninactivating currents. Thus, the hKv3.1-T400A and hKv2.1-T377A mutant behaved similarly, and the T to A mutation makes the channels noninactivating (Figs. 5 and 6).

Because elevating the extracellular [K^+] has been reported to accelerate U-type inactivation gating and to reduce conductivity (26,27), fast-switching K^+ titration experiments were performed with the aim of accelerating this process in hKv2.1-T377A. On the contrary, increasing extracellular [K^+] caused the current amplitude at +60 mV to increase (Fig. 7), although the effective K^+ driving force ($V_{effective} = V_{applied} - V_{reversal}$) decreased. To complement the results of the fast-switching K^+ titration experiments, the amount of steady-state voltage dependence of channel inactivation was determined at different extracellular [K^+] (Fig. 8). Similarly, upon elevated extracellular [K^+], the current amplitude of hKv2.1-T377A contradictorily increased. Thus, elevated extracellular [K^+] increases hKv2.1-T377A channels conductance instead of unmasking channel inactivation by accelerating this process as observed in WT hKv2.1 channels (Fig. S2). Another hallmark of increasing extracellular [K^+] is a gradual slowing of the deactivation kinetics. Determining the deactivation time constants of WT hKv2.1 and hKv2.1-T377A channels

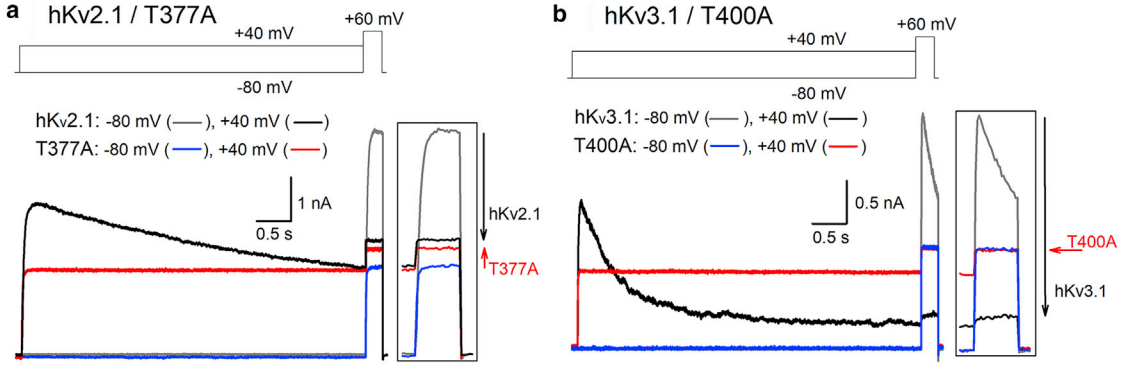

FIGURE 5 Effect of prolonged depolarization on the current amplitude. Panels show representative current recordings for WT hKv2.1 (*a*), WT hKv3.1 (*b*), and their corresponding hKv2.1-T377A and hKv3.1-T400A mutants. Current recordings were elicited with the pulse protocols shown on top. (*a*) A prolonged depolarization induces U-type inactivation in hKv2.1, which manifests as a time-dependent reduction in current amplitude (*black trace*). This decrease in current amplitude can be quantified by the current elicited during a subsequent test pulse at +60 mV, after a conditioning test pulse to +40 mV (*black trace*) or to −80 mV (*gray trace*). Inset on the right shows an enlarged view of the currents elicited during the test pulse to +60 mV. The magnitude of the current reduction during the test pulse at +60 mV is proportional to the size of the black arrow. For the mutant hKv2.1-T377A, the current amplitude slowly increased during membrane depolarization at +40 mV (*red trace*), noticeable by the increase in current amplitude (*red arrow*) during the +60 mV test pulse between a conditioning prepulse to −80 (*blue*) or +40 mV (*red*). (*b*) The current of WT hKv3.1, alike to hKv2.1, decreased in a time-dependent fashion upon prolonged depolarization at +40 mV (*black trace*). In contrast, hKv3.1-T400A did not display current reduction (*red trace*). Black arrow highlights, again, the amount of current reduction for WT hKv3.1 between a prepulse to −80 mV (*gray trace*) and +40 mV (*black trace*). The absence of current inactivation for hKv3.1-T400A between a prepulse to −80 mV (*blue*) and +40 mV (*red*) is indicated with the red arrow.

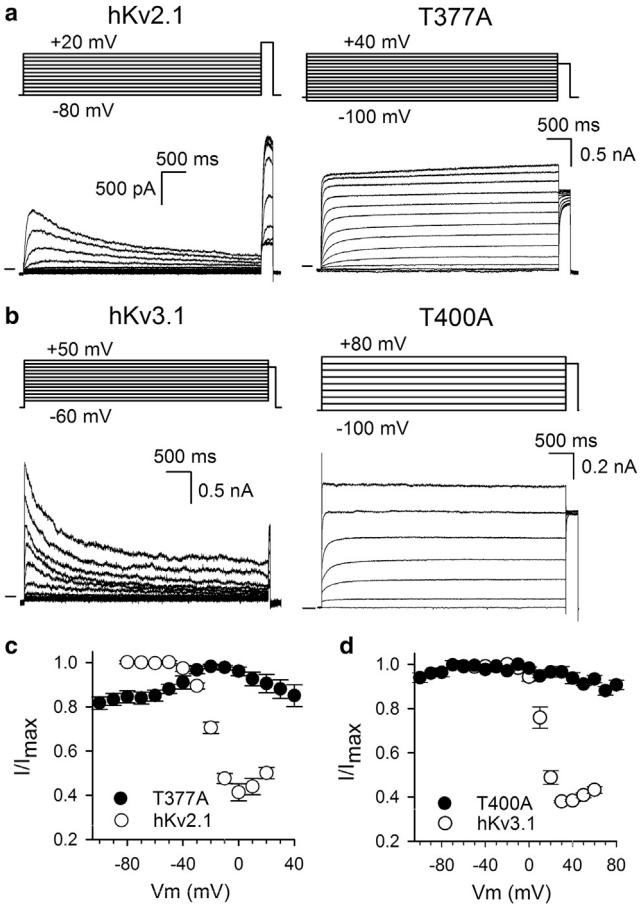

Figure360▷ FIGURE 6 For a Figure360 author presentation of this figure, see https://doi.org/10.1016/j.bpj.2020.03.032.

Inactivation kinetics of hKv2.1, hKv3.1 and their T-to-A mutants. (*a*) and (*b*) show representative current recordings for hKv2.1 (*a*) and hKv3.1 (*b*) channels with their T-to-A mutations represented on the right, respectively. Currents were elicited with the pulse protocols shown on top, and the zero-current level is indicated by the horizontal bar at the start of the recordings. Prolonged depolarizations induce inactivation in WT channels, resulting in a gradual decrease in current amplitude. The degree of channel inactivation was determined by applying an activating test pulse to +60 mV, which elicited a current amplitude that reports directly on the number of channels that did not inactivate. Note, the current amplitude of hKv2.1-T377A (*a*) gradually increased upon prolonged depolarization or remained constant for hKv3.1-T400A (*b*). (*c*) and (*d*) display the voltage dependence of channel inactivation for the WT hKv2.1 and hKv3.1 channels (*open circles*). Curves were obtained by plotting the normalized current amplitude at the +60 mV test pulse at (I/Imax) as a function of the 5-s preconditioning depolarization. Stronger depolarizations induced after 5 s ~60 and 70% of channel inactivation in hKv2.1 (*c*) and hKv3.1 (*d*), respectively. Plotting the normalized currents elicited with the activating test pulse for the T-to-A mutations (*solid circles*) resulted in an opposite behavior. The mutants did not inactivate, and hKv2.1-T377A contradictorily displayed an increase in current (*c*). Represented values are the means ± SEM from five to eight independent observations.

indicated a similar slowing of channel closure upon increasing extracellular [K^+] (Fig. S3). The fully open IV curves of both WT hKv2.1 and the hKv2.1-T377A behaved as expected with a loss of rectification and a shift of the reversal potential (Fig. S3). To explore whether the hKv3.1-T400A mutant behaved similarly, K^+ titration experiments were performed and the extracellular [K^+] was changed from low (4 mM) to high (148 mM). Although at +40 mV depolarization, the net driving force falls with increased extracellular [K^+], a slight increase in hKv3.1-T400A current was observed (Figs. 7 and 8). The fully open IV curves and channel deactivation kinetics responded in WT hKv3.1 and hKv3.1-T400A similarly upon gradually increased extracellular [K^+] (Fig. S4). Thus, hKv3.1-T400A behaved like hKv2.1-T377A, and interestingly, both displayed a similar behavior as reported for the T to A mutations in *Shaker* and hKv1.5 (25).

DISCUSSION

Replacing the second threonine of the conserved TTVGYG sequence in the SF of the *Shaker* and the hKv1.5 channel with an alanine inverted the coupling between AG opening and SF inactivation (25). Introducing the equivalent mutation in hKv2.1 and hKv3.1 yielded functional voltage-dependent hKv2.1-T377A and hKv3.1-T400A channels. Interestingly, whereas the T to A mutation is believed to eliminate the fourth K^+ binding site, both Kv2.1-T377A and Kv3.1-T400A remained highly selective for K^+ over Na^+. However, the channel's unitary conduction was reduced, which is most likely due to a reduction (elimination) of normal ion occupancy at the fourth K^+ binding site, as evidenced by crystallography of the equivalent T to A mutation in KcsA (T75A) (25). The conservation of ion selectivity combined with a lower single-channel conductance is similar to what has been reported for the homologous mutants in *Shaker* and hKv1.5.

By mutating T377 and T400 to an alanine in the hKv2.1 and hKv3.1 channels, we aimed to investigate the role of the intracellular side of the SF in U-type inactivation gating. In both channels, the T by A substitution affected the inactivation profile and neither hKv2.1-T377A nor hKv3.1-T400A displayed inactivation upon prolonged 5-s depolarizations, conditions that causes WT hKv2.1 and WT hKv3.1 to inactivate (Fig. 6). Whereas the homologous T to A mutation in *Shaker*-type channels inverted the coupling between the AG and SF, both hKv2.1-T377A and hKv3.1-T400A did not display obvious inactivation when the channel gate closed (i.e., closed-state inactivation) (Fig. S1). However, in hKv2.1-T377A there was the notion that moderate depolarizations resulted in an increase in current, followed by a reduction at stronger depolarizations (Fig. 6). Although the effect is small, it indicates that the hKv2.1-T377A channel adopts a higher conductance state upon channel gate opening instead of inactivating. This could mean that hKv2.1-T377A channels do adopt a kind of closed-inactivated state when the channel gate is closed, and membrane depolarization recruits them to their higher conductive state, in analogy with the T to A mutations in *Shaker* and hKv1.5. Alternatively, the reorientations associated with inactivation of WT channels are

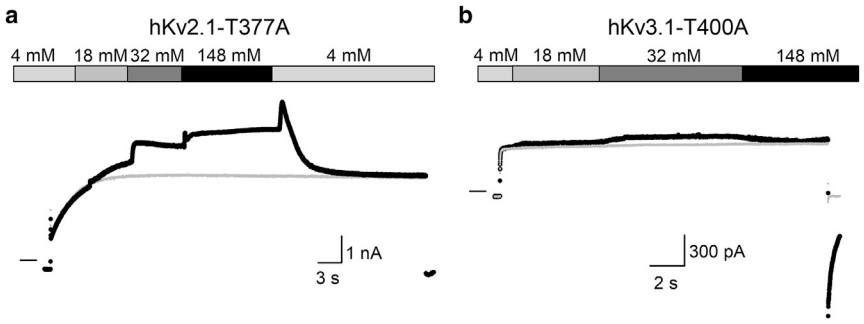

FIGURE 7 Increased external K^+ results in larger macroscopic currents in hKv2.1-T377A and hKv3.1-T400A. (*a*) A representative hKv2.1-T377A recording showing the effect of increasing the external K^+ concentration on current amplitude using a pressurized fast perfusion system. During a prolonged depolarization to +40 mV, starting from −80-mV holding potential, the external K^+ concentration was changed gradually from 4 to 148 mM, as indicated on top. Elevating the external K^+ concentration increased T377A current amplitude; despite that, the outward directed electrochemical driving force for K^+ is reduced. Switching the extracellular K^+ concentration back to 4 mM resulted in a transient increase in amplitude, which is in agreement with a stronger outward electrochemical driving force, followed by a current decrease. The gray line represents the current recorded in standard 4 mM extracellular solution. Horizontal bar at the start of the recording indicates the zero-current level. (*b*) A representative current recording for hKv3.1-T400A upon increasing gradually the extracellular K^+ concentration is shown.

present in hKv2.1-T377A, but instead of making the channels non- or less conductive, as in WT, the conductivity increases. Nevertheless, the observation that substituting the second threonine of the conserved TTVGYG sequence in the SF with alanine makes the Kv2.1 and Kv3.1 channels resistant to inactivation suggests that this residue is involved in the U-type inactivation process of these channels.

A reported hallmark of C-type inactivation is that this mechanism is modified by external $[K^+]$ (31–33). In case of the equivalent T to A mutations in *Shaker* and hKv1.5, recovering the SF from its closed-inactivated state was accelerated by increasing external $[K^+]$. Although for U-type (low voltage induced) inactivation, an opposite response to elevated external $[K^+]$ has been reported compared with C-type inactivation (26,27), the recovery from inactivation is reported to be accelerated by elevated extracellular $[K^+]$, as in C-type inactivation (27,36). The hKv2.1-T377A and hKv3.1-T400A mutant behaved similarly, and increased external $[K^+]$ prompted the hKv2.1-T377A and hKv3.1-T400A channels to adopt a higher conductive state. It has been reported that a moderate elevation of external $[K^+]$ increases the conductance in WT

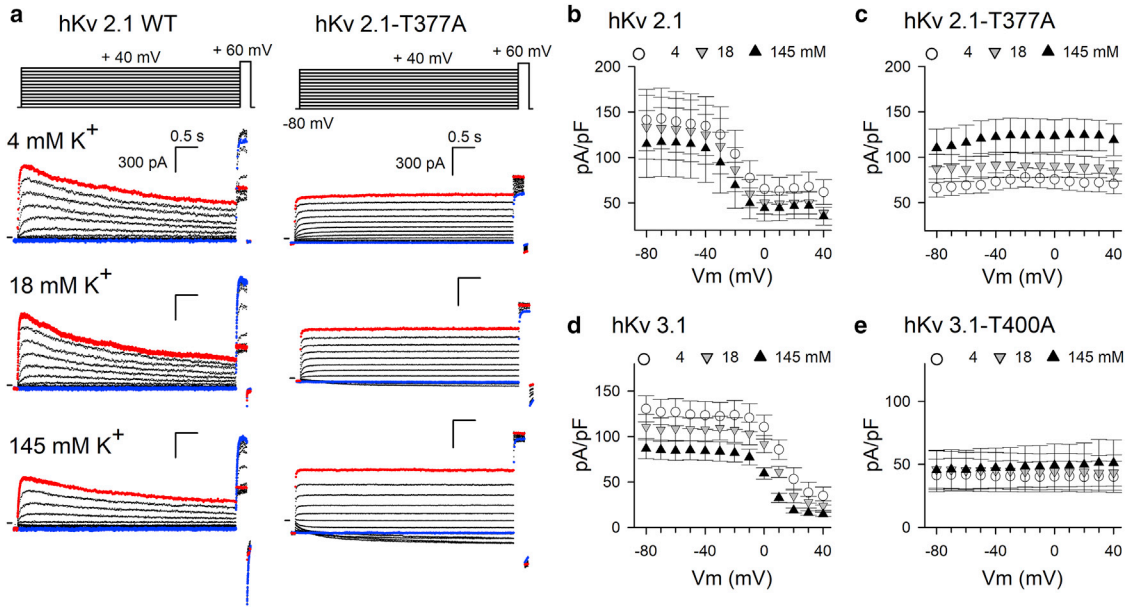

FIGURE 8 Elevated external K^+ increases current amplitude in hKv2.1-T377A and hKv3.1-T400A channels. (*a*) shows example recordings from WT Kv2.1 and Kv2.1-T377A, using the pulse protocol on top and in three different external $[K^+]$. (*b*) and (*d*) show the current density at a +60-mV test pulse as a function of the conditioning 5-s prepulse potential for the WT hKv2.1 ($n = 3$) and hKv3.1 ($n = 3$) channels, (*c*) and (*e*) for hKv2.1-T377A ($n = 3$), and hKv3.1-T400A ($n = 3$), respectively. Represented values are the means ± SEM. Although both WT channels clearly demonstrate inactivation, U-type inactivation is only observed for hKv2.1. Stronger depolarizations are necessary to reveal U-type inactivation in hKv3.1. Increasing the extracellular $[K^+]$ reduces the current density at +60 mV. The hKv2.1-T377A mutant lacks inactivation and even displays an initial increase in current density at 4 mM (*white circles*) and 18 mM (*gray inverted triangles*) external $[K^+]$. Moreover, the current amplitude of hKv2.1-T377A increased with elevated external $[K^+]$ and was largest with 145 mM external $[K^+]$ (*black triangles*). Similar to hKv2.1-T377A, there is no decrease in current amplitude for hKv3.1-T400A with elevated external $[K^+]$ (*d*), as is the case for the WT hKv3.1 channel (*c*).

hKv2.1 by recruiting the channels from a low-conductive state (43,44). However, current amplitudes start to decrease at concentrations above 10 mM because of a reduction in the electrochemical driving force. It is possible that this "beneficial" K^+ effect on conductivity can, in the hKv2.1-T377A, be shifted toward higher K^+ concentrations or be amplified by the absence of channel inactivation. Alternatively, external [K^+]-dependent reorientations that affect inactivation in WT channels occur in the T to A mutants but cause the macroscopic current levels to increase. Although there is no direct evidence of changes in ion selectivity, we propose an involvement of the SF in the external [K^+]-dependent increase of channel conductance in both hKv2.1-T377A and hKv3.1-T400A, as is reported for the homologous T to A mutations in *Shaker*-type channels (25).

Within the *Shaker* channel, it is reported that SF inactivation affects the activation and deactivation process (35). Thus, communication between AG and SF structure seems bidirectional (24). If such an SF and activation gate communication exists in hKv2.1 and hKv3.1, then the shifted voltage dependence of channel activation in hKv2.1-T377A and the combined shift in activation with slowed deactivation kinetics of hKv3.1-T400A can be explained by mutation-induced reorientations of the SF that makes it resistant to inactivate but promotes channel gate opening, comparable to what was previously reported for the homologous mutants in *Shaker* and hKv1.5 channels (25). Interestingly, the deactivation kinetics of hKv2.1-T377A and hKv3.1-T400A slowed down gradually with increasing extracellular [K^+], similar to the response of the WT channels (Fig. S3). If this slowing in gate closure is due to a communication between SF reorientations and gate movements, as in *Shaker*-type channels, then the communication between SF and gate is maintained in the hKv2.1-T377A and hKv3.1-T400A channels. The question remains whether the observed extracellular [K^+]-dependent increase in conductance is due to the reorientations of the SF or to that of other regions within the pore domain, such as the channel gate (45).

Whereas the A for T substitution in the *Shaker* and hKv1.5 resulted in channels that recovered from a low- or nonconductive state upon gate opening, a closed-inactivated state was not obvious in the hKv2.1-T377A and the hKv3.1-T400A channel. However, in both hKv2.1 and hKv3.1, the T to A mutation affects the inactivation process substantially. This is not the case for the homologous *Shaker* T449 substitution in Kv2.1 (residue Y380, respectively), which is reported to have no effect on Kv2.1's inactivation process, whereas T449 is well reported to affect inactivation in *Shaker* (33,46). The homologous residue in also hKv1.5 does not appear critical for regulating the speed of inactivation (47). Because T449 in *Shaker* and its homologous counterparts in Kv1.5 and Kv2.1 localize at the extracellular side of the SF, this residue possibly affects the outer most K^+ binding site of the SF. The second threonine residue of the TTVGYG motif studied in here is located at the intracellular side of the SF, and the mutation of this residue into an alanine seems to affect both the C- and U-type inactivation process.

In conclusion, hKv2.1-T377A and hKv3.1-T400A are channels that do not inactivate, and elevating the extracellular [K^+] increased the conductivity. Although the activation process involves reorientations within the VSDs, the S4–S5 linker, S5, outer pore mouth, and P-loop, which, through a plenitude of interactions with a possible contribution of the N- and C-termini, can modulate the U-type inactivation process (48–51), our data highlight the intracellular side of the SF as an important determinant of U-type inactivation. By extension, the presented data support the idea of the existence of an allosteric coupling between AG and SF gating, as is the case of channels that display C-type inactivation.

SUPPORTING MATERIAL

Supporting Material can be found online at https://doi.org/10.1016/j.bpj.2020.03.032.

AUTHOR CONTRIBUTIONS

L.C., E.M., N.D.N., and A.J.L. performed research. L.G.C. and A.J.L. designed research. L.C., N.D.N., and A.J.L. analyzed data. L.C., D.J.S., L.G.C., and A.J.L. interpreted results and wrote the article.

ACKNOWLEDGMENTS

A.J.L., L.C., and D.J.S. thank A. Van Tilborg for excellent technical support.

This work was supported by the University Research Fund of the University of Antwerp (BOF DOCPRO PhD funding to L.C.). L.G.C. was supported by research grant National Institutes of Health 2R01GM097159.

REFERENCES

1. Hille, B. 2001. Ion Channels of Excitable Membranes, Third Edition. Sinauer, Sunderland, MA.
2. Gutman, G. A., K. G. Chandy, …, X. Wang. 2005. International union of pharmacology. LIII. Nomenclature and molecular relationships of voltage-gated potassium channels. *Pharmacol. Rev.* 57:473–508.
3. Cuello, L. G., D. M. Cortes, and E. Perozo. 2017. The gating cycle of a K^+ channel at atomic resolution. *eLife.* 6:e28032.
4. Long, S. B., E. B. Campbell, and R. Mackinnon. 2005. Crystal structure of a mammalian voltage-dependent *Shaker* family K^+ channel. *Science.* 309:897–903.
5. Heginbotham, L., Z. Lu, …, R. MacKinnon. 1994. Mutations in the K^+ channel signature sequence. *Biophys. J.* 66:1061–1067.
6. Doyle, D. A., J. Morais Cabral, …, R. MacKinnon. 1998. The structure of the potassium channel: molecular basis of K^+ conduction and selectivity. *Science.* 280:69–77.
7. Labro, A. J., and D. J. Snyders. 2012. Being flexible: the voltage-controllable activation gate of kv channels. *Front. Pharmacol.* 3:168.
8. Kalstrup, T., and R. Blunck. 2013. Dynamics of internal pore opening in K(V) channels probed by a fluorescent unnatural amino acid. *Proc. Natl. Acad. Sci. USA.* 110:8272–8277.

9. Blunck, R., and Z. Batulan. 2012. Mechanism of electromechanical coupling in voltage-gated potassium channels. *Front. Pharmacol.* 3:166.
10. Blunck, R., J. F. Cordero-Morales, …, F. Bezanilla. 2006. Detection of the opening of the bundle crossing in KcsA with fluorescence lifetime spectroscopy reveals the existence of two gates for ion conduction. *J. Gen. Physiol.* 128:569–581.
11. Hoshi, T., W. N. Zagotta, and R. W. Aldrich. 1991. Two types of inactivation in *Shaker* K^+ channels: effects of alterations in the carboxy-terminal region. *Neuron.* 7:547–556.
12. Cordero-Morales, J. F., L. G. Cuello, …, E. Perozo. 2006. Molecular determinants of gating at the potassium-channel selectivity filter. *Nat. Struct. Mol. Biol.* 13:311–318.
13. Cuello, L. G., V. Jogini, …, E. Perozo. 2010. Structural mechanism of C-type inactivation in K(+) channels. *Nature.* 466:203–208.
14. Li, J., J. Ostmeyer, …, B. Roux. 2018. Rapid constriction of the selectivity filter underlies C-type inactivation in the KcsA potassium channel. *J. Gen. Physiol.* 150:1408–1420.
15. Liu, Y., M. E. Jurman, and G. Yellen. 1996. Dynamic rearrangement of the outer mouth of a K^+ channel during gating. *Neuron.* 16:859–867.
16. Pau, V., Y. Zhou, …, Z. Lu. 2017. Crystal structure of an inactivated mutant mammalian voltage-gated K^+ channel. *Nat. Struct. Mol. Biol.* 24:857–865.
17. Ben-Abu, Y., Y. Zhou, …, O. Yifrach. 2009. Inverse coupling in leak and voltage-activated K+ channel gates underlies distinct roles in electrical signaling. *Nat. Struct. Mol. Biol.* 16:71–79.
18. Cuello, L. G., V. Jogini, …, E. Perozo. 2010. Structural basis for the coupling between activation and inactivation gates in K(+) channels. *Nature.* 466:272–275.
19. Pan, A. C., L. G. Cuello, …, B. Roux. 2011. Thermodynamic coupling between activation and inactivation gating in potassium channels revealed by free energy molecular dynamics simulations. *J. Gen. Physiol.* 138:571–580.
20. Panyi, G., and C. Deutsch. 2006. Cross talk between activation and slow inactivation gates of Shaker potassium channels. *J. Gen. Physiol.* 128:547–559.
21. Peters, C. J., D. Fedida, and E. A. Accili. 2013. Allosteric coupling of the inner activation gate to the outer pore of a potassium channel. *Sci. Rep.* 3:3025.
22. Sadovsky, E., and O. Yifrach. 2007. Principles underlying energetic coupling along an allosteric communication trajectory of a voltage-activated K+ channel. *Proc. Natl. Acad. Sci. USA.* 104:19813–19818.
23. Kalstrup, T., and R. Blunck. 2018. S4-S5 linker movement during activation and inactivation in voltage-gated K^+ channels. *Proc. Natl. Acad. Sci. USA.* 115:E6751–E6759.
24. Tilegenova, C., D. M. Cortes, and L. G. Cuello. 2017. Hysteresis of KcsA potassium channel's activation- deactivation gating is caused by structural changes at the channel's selectivity filter. *Proc. Natl. Acad. Sci. USA.* 114:3234–3239.
25. Labro, A. J., D. M. Cortes, …, L. G. Cuello. 2018. Inverted allosteric coupling between activation and inactivation gates in K^+ channels. *Proc. Natl. Acad. Sci. USA.* 115:5426–5431.
26. Klemic, K. G., G. E. Kirsch, and S. W. Jones. 2001. U-type inactivation of Kv3.1 and Shaker potassium channels. *Biophys. J.* 81:814–826.
27. Klemic, K. G., C. C. Shieh, …, S. W. Jones. 1998. Inactivation of Kv2.1 potassium channels. *Biophys. J.* 74:1779–1789.
28. Kurata, H. T., G. S. Soon, …, D. Fedida. 2002. Amino-terminal determinants of U-type inactivation of voltage-gated K^+ channels. *J. Biol. Chem.* 277:29045–29053.
29. Jamieson, Q., and S. W. Jones. 2014. Shaker IR T449 mutants separate C- from U-type inactivation. *J. Membr. Biol.* 247:319–330.
30. Kurata, H. T., K. W. Doerksen, …, D. Fedida. 2005. Separation of P/C- and U-type inactivation pathways in Kv1.5 potassium channels. *J. Physiol.* 568:31–46.
31. Baukrowitz, T., and G. Yellen. 1995. Modulation of K^+ current by frequency and external $[K^+]$: a tale of two inactivation mechanisms. *Neuron.* 15:951–960.
32. Baukrowitz, T., and G. Yellen. 1996. Use-dependent blockers and exit rate of the last ion from the multi-ion pore of a K^+ channel. *Science.* 271:653–656.
33. López-Barneo, J., T. Hoshi, …, R. W. Aldrich. 1993. Effects of external cations and mutations in the pore region on C-type inactivation of *Shaker* potassium channels. *Receptors Channels.* 1:61–71.
34. Kiss, L., J. LoTurco, and S. J. Korn. 1999. Contribution of the selectivity filter to inactivation in potassium channels. *Biophys. J.* 76:253–263.
35. Starkus, J. G., L. Kuschel, …, S. H. Heinemann. 1997. Ion conduction through C-type inactivated *Shaker* channels. *J. Gen. Physiol.* 110:539–550.
36. Levy, D. I., and C. Deutsch. 1996. Recovery from C-type inactivation is modulated by extracellular potassium. *Biophys. J.* 70:798–805.
37. Kiss, L., and S. J. Korn. 1998. Modulation of C-type inactivation by K+ at the potassium channel selectivity filter. *Biophys. J.* 74:1840–1849.
38. Aiyar, J., A. N. Nguyen, …, S. Grissmer. 1994. The P-region and S6 of Kv3.1 contribute to the formation of the ion conduction pathway. *Biophys. J.* 67:2261–2264.
39. Chapman, M. L., H. S. Krovetz, and A. M. VanDongen. 2001. GYGD pore motifs in neighbouring potassium channel subunits interact to determine ion selectivity. *J. Physiol.* 530:21–33.
40. Hartmann, H. A., G. E. Kirsch, …, A. M. Brown. 1991. Exchange of conduction pathways between two related K^+ channels. *Science.* 251:942–944.
41. Kanemasa, T., L. Gan, …, L. K. Kaczmarek. 1995. Electrophysiological and pharmacological characterization of a mammalian Shaw channel expressed in NIH 3T3 fibroblasts. *J. Neurophysiol.* 74:207–217.
42. Pascual, J. M., C. C. Shieh, …, A. M. Brown. 1997. Contribution of the NH2 terminus of Kv2.1 to channel activation. *Am. J. Physiol.* 273:C1849–C1858.
43. Trapani, J. G., P. Andalib, …, S. J. Korn. 2006. Control of single channel conductance in the outer vestibule of the Kv2.1 potassium channel. *J. Gen. Physiol.* 128:231–246.
44. Wood, M. J., and S. J. Korn. 2000. Two mechanisms of K(+)-dependent potentiation in Kv2.1 potassium channels. *Biophys. J.* 79:2535–2546.
45. Díaz-Franulic, I., R. V. Sepúlveda, …, D. Naranjo. 2015. Pore dimensions and the role of occupancy in unitary conductance of Shaker K channels. *J. Gen. Physiol.* 146:133–146.
46. Jamieson, Q., and S. W. Jones. 2013. Role of outer-pore residue Y380 in U-type inactivation of KV2.1 channels. *J. Membr. Biol.* 246:633–645.
47. Fedida, D., N. D. Maruoka, and S. Lin. 1999. Modulation of slow inactivation in human cardiac Kv1.5 channels by extra- and intracellular permeant cations. *J. Physiol.* 515:315–329.
48. Cheng, Y. M., J. Azer, …, T. W. Claydon. 2011. Molecular determinants of U-type inactivation in Kv2.1 channels. *Biophys. J.* 101:651–661.
49. Immke, D., M. Wood, …, S. J. Korn. 1999. Potassium-dependent changes in the conformation of the Kv2.1 potassium channel pore. *J. Gen. Physiol.* 113:819–836.
50. Kurata, H. T., and D. Fedida. 2006. A structural interpretation of voltage-gated potassium channel inactivation. *Prog. Biophys. Mol. Biol.* 92:185–208.
51. VanDongen, A. M., G. C. Frech, …, A. M. Brown. 1990. Alteration and restoration of K^+ channel function by deletions at the N- and C-termini. *Neuron.* 5:433–443.